Absorption Spectroscopy Based High-Speed Oxygen Concentration Measurements at Elevated Gas Temperatures

Gurneesh S. Jatana[1], Anthony K. Perfetto[2], Samuel C. Geckler[2], and William P. Partridge[1]*
[1]Fuels, Engines and Emissions Research Center, Oak Ridge National Lab, USA
[2]Cummins Inc., Columbus - IN, USA
[*]Corresponding Author Email: partridgewp @ornl.gov

Abstract: A sensor based on tunable diode laser absorption spectroscopy (TDLAS) has been developed for concentration measurements in high-temperature (up to 800 K) gas streams; while the sensor measures gas oxygen and water concentration, temperature and pressure, this work focuses on the challenges and solutions to transient oxygen measurement. A 760-nm diode laser was used to probe a pair of oxygen absorption transitions, and a Herriott cell based multi-pass arrangement was utilized to compensate for the extremely weak oxygen absorption as well as the high gas temperature. This multi-pass arrangement provides a 4297.4-mm absorption path length across a 76.2-mm diameter duct, and an O_2 detection limit ($[O_2]$ where SNR=1) of ca. 0.1 %. Laboratory validation of the HITRAN spectral parameters of the chosen absorption transitions was performed over a range of high temperatures and oxygen concentrations relevant to engine-exhaust applications. The insensitivity of the Herriott cell arrangement to vibrations and spatial temperature gradients was demonstrated. Results from applications to single- and multi-cylinder engine exhaust are presented and demonstrate the new sensor's ability to measure fast intra-cycle gas-property transients, and provide insights relevant to advancing internal-combustion-engine technology.

Keywords: Oxygen, Herriott-Cell, Absorption, High-Speed, Water Vapor, High-Temperature

1. Introduction

Molecular oxygen is the primary oxidizer in air-breathing combustion systems such as internal combustion (IC) engines, burners, gas turbine engines and ramjet combustors. Measurements of oxygen concentration in the combustion products not only provide insights into the quality of combustion, but provides a quantifiable figure of merit for assessing and developing strategies to improve combustion efficiency and stability. In IC engine applications, near-crank-angle-resolved exhaust oxygen concentration measurements could identify potential air-to-fuel ratio (AFR) variations; specifically, from cycle to cycle for a given engine cylinder (cylinder-specific variations), as well as across the different cylinders within a given cycle (cycle-specific variations). Such AFR variations result from the engine fueling and/or air-flow differing from the value commanded by the engine controller; typically, due to hysteresis and offsets in the throttle and injector operation [1]. These variations mandate greater engineering margins, and conservative and less efficient engine control strategies to prevent excess engine-out emissions and vibrations, and result in suboptimal engine performance. The detection and characterization of these variations is critical to developing and fine-tuning engine control models necessary to reduce engine-out emissions and improve combustion efficiency.

Detection of exhaust O_2 concentration ($[O_2]$) variations on an engine cycle- and cylinder-specific basis requires O_2 measurements at a near-crank-angle resolution. The multi-kHz bandwidth required for crank-angle-scale measurements cannot be provided by the sampling gas analyzers (e.g., paramagnetic detectors, around 1 Hz) or by the wideband oxygen sensors (up to 50 Hz) [2]. Therefore, an advanced sensor based on diode-laser absorption spectroscopy has been developed and applied to perform high-speed (up to 5 kHz; 1.2 CAD at 1000 RPM) measurements of $[O_2]$ in the exhaust of IC engines. This new sensor builds upon and adds to the

previously reported sensor development for high-speed gas temperature (T), pressure (P), and H_2O concentration ([H_2O]) measurements in IC-engine intake and exhaust manifolds [3,4].

Laser-based absorption spectroscopy is a quantitative and species-specific technique that measures path-averaged gas properties along the laser-absorption path, and has been extensively used for gas property measurements in IC engines [3-10], as well as in various other combustion systems such as gas turbine engines [11], scramjet combustors [12], and laboratory flat-flame burners [13]. A single-pass line-of-sight arrangement of a 1388-nm distributed-feedback diode laser utilizes absorption by water vapor to determine gas T, P, and [H_2O]. Water vapor absorption spectroscopy near 1388 nm as well as the data analysis to extract gas property information from absorption measurements has already been demonstrated in literature [3-5]. For fast, absorption-based oxygen measurements, the major absorption band is near 760 nm. Because the absorption cross-sections of these oxygen lines are ~100 times weaker than the target water vapor lines, a short mm-to-cm scale absorption pathlength as used for the H_2O measurements is not practically possible for fast O_2 measurements. To accommodate the weaker O_2 absorption and the need for high-speed measurements, a multi-pass Herriott cell [14, 15] arrangement was implemented to provide a 4297.4-mm absorption path length across a 3-in (76.2-mm) inside diameter (ID) measurement duct. Multiple instances of oxygen absorption measurements have previously been described in literature [16-21]. Schlosser et al. [16] demonstrated a Herriott cell based O_2 absorption sensor for *in situ* oxygen measurements under fire-suppression conditions with large and rapid obscuration changes. However, the Herriot cell setup was designed for room-scale applications and provided only 1800-mm absorption path length for a Herriot cell mirror spacing of 300 mm at a measurement rate of 2.5 Hz. Zhang et al. [17] demonstrated the use of oxygen absorption spectroscopy for gas T measurements in a heated gas cell. Other implementations of oxygen absorption spectroscopy found in literature were also limited to laboratory-grade gas cells, and there have been no reports of a sensor system capable of on-engine measurements on a production multi-cylinder IC engine. Furthermore, no prior data was found for the specific oxygen absorption transition utilized in this study.

This study describes development of a new sensor for quantifying fast IC-engine-exhaust transients in [O_2] and [H_2O], T and P using line-of-sight absorption-based measurements. While the full sensor is described and evaluated, the primary focus is on challenges of the O_2 measurements. The multi-pass Heriott cell configuration is described, and its robust performance in conditions of harsh engine vibrations is demonstrated. Sensitivity of the Herriott cell to exhaust deposits is evaluated, and mitigation strategies are described and evaluated. The validity of the spectral parameters of the chosen O_2 absorption transitions is demonstrated for the high-temperature gas conditions expected in IC-engine exhaust, and the accuracy of the overall O_2 sensor is demonstrated. Furthermore, the instrument is applied for exhaust measurements on an operating IC engine, which demonstrates the temporal resolution and sensitivity necessary for advancing the motivating goals; enabling the study of cylinder-to-cylinder AFR variations, cylinder-specific fuel tuning, advanced fuel-control strategies for improved combustion uniformity, and more generally for advancing IC-engine technology.

2. Absorption Theory

Laser absorption spectroscopy is a quantitative, species specific, and path-averaged non-intrusive technique that can be used to measure gas T, P and species concentration

simultaneously in a medium through which the laser radiation is transmitted and interacts. For a fixed set of medium properties (P, T, and absorbing species concentration), maximum absorption occurs when the incident laser radiation frequency matches the resonance frequency (single-photon transition between low- and high-energy levels) of the absorbing species. For a monochromatic laser source, this resonant absorption process can be described by the Beer-Lambert relation

$$\frac{I_L}{I_o} = \exp\left(-k_\nu * L\right), \tag{1}$$

where I_o and I_L are the incident and transmitted laser intensities [W·cm^{-2}] respectively, L [cm] is the absorption path length, k_ν [cm^{-1}] is the single-transition spectral absorption coefficient, and ν [cm^{-1}] is the laser light frequency. The absorption coefficient can be represented by

$$k_\nu = P * X * S\left(T\right) * \phi_V , \tag{2}$$

where P [atm] is the medium pressure, ϕ_V [cm] is the Voigt line shape function, X is the absorbing species mole fraction, and $S(T)$ [cm^{-2}·atm^{-1}] is the line-strength of the transition at temperature T [K]. As detailed in previous work [3], the relative height of two or more absorption-transition peaks is the main source of temperature sensitivity in the absorption signal; while the pressure and concentration information is embedded both in the Voigt line shape profile through the collisional broadening half-width ($\Delta\nu_C$ [cm^{-1}] in Eq. 3) as well as the partial pressure of the absorbing species. The collisional broadening half-width is given by

$$\Delta\nu_C = 2 * P * \sum_i X_i \gamma_i , \tag{3}$$

where γ_i [cm^{-1}·atm^{-1}] is the temperature-dependent collisional broadening coefficient. Through this set of relations and the associated spectroscopic parameters and measurements, all target gas properties (i.e. gas T, gas P, and absorbing species concentration) can be extracted from the absorption signal by recording multiple absorption features.

In this study, the gas T, P, and [H_2O] measurements were performed using H_2O absorption transitions in the 7201-7206 cm^{-1} spectral region and the HITRAN 2004 [22] based spectral parameters for these transitions have already been validated in literature [23] for gas temperatures up to 1000 K. The [O_2] measurements were performed using the transition-doublet near 13158 cm^{-1} (in the 0-0 band of the $^1\Sigma_g^+ \leftarrow {}^3\Sigma_g^-$ electronic system [24]) as this transition maintains a relatively stronger absorption cross-section at high temperature while remaining free from water-absorption interferences at high gas temperatures. Spectral parameters for the selected H_2O and O_2 transitions are listed in **Table 1**. The performance of the HITRAN 2012 [25] O_2 absorption spectral parameters used in this study is validated at the expected IC-engine exhaust gas conditions in Section 3 below.

Table 1: Spectroscopic details for the selected H_2O [22] and O_2 [25] absorption transitions.

Line Number	Transition Frequency (cm^{-1})	Line Strength (296K) (cm^{-2}·atm^{-1})	Rotational Quantum Numbers (J, K_a, K_c)		Vibrational Quantum Numbers (v_1, v_2, v_3)		Lower State Energy (cm^{-1})
			Upper	Lower	Upper	Lower	
H_2O_1	7202.26	2.52E-02	(5,2,4)	(5,2,3)	(1,0,1)	(0,0,0)	446.51
H_2O_2	7202.91	1.15E-01	(1,0,1)	(2,0,2)	(1,0,1)	(0,0,0)	70.09

H_2O_3	7203.66	1.49E-04	(2,2,0)	(2,2,1)	(1,1,1)	(0,1,0)	1742.31
H_2O_4	7203.89	7.38E-02	(5,5,1)	(5,5,0)	(1,0,1)	(0,0,0)	742.08
H_2O_5	7204.17	7.85E-03	(7,4,4)	(7,4,3)	(1,0,1)	(0,0,0)	931.24
H_2O_6	7205.25	2.46E-01	(1,1,1)	(2,1,2)	(1,0,1)	(0,0,0)	79.50
O_2_1	13158.68	5.14E-4	-	-	-	-	546.7
O_2_2	13158.74	8.38E-4	-	-	-	-	438.44

3. Validation of Spectral Parameters of the O_2 Absorption Transitions

Spectral parameters listed in the HITRAN 2012 spectral database were utilized for processing O_2 absorption data from high-temperature engine exhaust. The HITRAN parameters are typically applicable for near-ambient (296 K) temperatures and are generally listed with a 5% uncertainty. To increase confidence regarding use of these parameters at elevated gas temperatures typical of IC-engine exhaust, the spectral parameters were validated in a high-temperature gas cell using a bottled standard mixture of 20-% O_2 and 80-% N_2 while the gas temperature was swept from 300 K to 800 K in 50-K steps. The 400-mm long heated cell [5] featured recessed windows resulting in a line-of-sight absorption path length of ~100 mm in the cell center. This design reduced T gradients along the absorption path length, which was monitored via four uniformly distributed thermocouples (Omega SCASS-020U-12); the four thermocouples measured within 2 % of each other, indicating effectively uniform gas T along the absorption path. To improve the signal-to-noise ratio of the oxygen absorption signal for the validation experiments, a simple multi-pass arrangement was implemented by replacing one of the heated-cell windows with a silver-coated flat mirror. A second mirror was positioned outside the cell to arrange two round-trip passes of the laser beam within the cell. The exact path-length of this multi-pass arrangement was determined to be 462 mm by comparing ambient O_2 absorption measurements in the multi-pass cell with single-pass line-of-sight measurements performed across a known path length. Use of N_2 purging prevented absorption of laser light by ambient O_2 outside the gas cell absorption path. Figure 1 shows the good quality of O_2 spectral fits achieved using the HITRAN 2012 parameters across the measured high-temperature range; this goodness of fit is evidence of the validity of the spectral parameters for high-temperature IC-engine exhaust applications in this range.

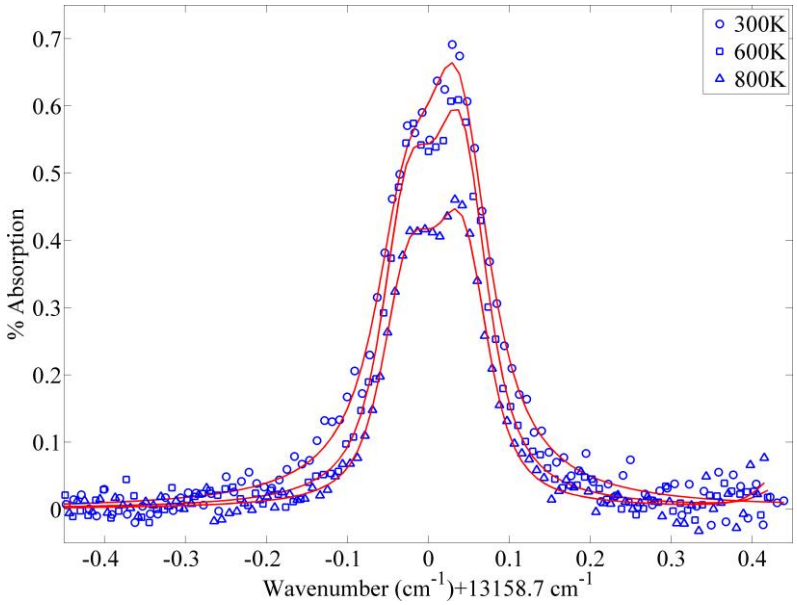

Figure 1: Experimental absorption data (blue markers) and the associated spectral fits (red lines) for 20-% O_2 in N_2 at gas temperature of 300 K, 600 K, and 800 K. The spectral fits match well with the experimental data.

Further assessment of the HITRAN 2012 O_2 spectroscopic parameters across IC-engine exhaust temperatures in terms of calculated [O_2] required accounting for signal contributions from etalons. Etalons resulting from multiple-beam interference from reflections of the swept-wavelength laser source off parallel surfaces in the optical train can create spectrally structured signal that complicates analysis of O_2 absorption spectra. Indeed, etalons were detected under non-absorbing conditions (100-% N_2) in the transmitted laser light from the heated cell used for spectroscopic parameter validation; the etalons were attributed to a combination of the multi-pass arrangement and the uncoated window used in this study. To alleviate the impact of etalons on the validation results, a background trace was recorded at each temperature while a Zero gas (100-% N_2) was passed through the cell. Subsequently, the gas supply was switched to the Reference gas (20-% O_2 and 80-% N_2) for absorption measurement, and the Zero-gas background trace was subtracted prior to spectral analysis. However, slight changes in the thermal equilibrium were observed when switching from the Zero to Reference gas, resulting in changes in the etalon profile; while the Zero-gas background subtraction accounted for the major etalon signal contributions, the unavoidable thermal equilibrium variations associated with gas switching produced smaller nominally random etalon signal contribution. To mitigate the random component from the etalon correction, validation measurements were performed for six independent T sweeps and results were averaged. This averaged etalon-corrected analysis allows the high-temperature effects via the spectral parameter values on [O_2] measurements to be isolated and quantified. Figure 2 shows the results, which match the 20-% O_2 Reference value very well (within 5 %) across the full high-temperature range. A standard deviation of 3 % was observed among the mean values of the six temperature sweeps, while within each sweep at a given T, a standard deviation of only 1 % was observed at 20-% O_2; the higher (3 %) standard deviation in-between the six sweeps is a result of residual etalon influence, while the lower (1 %) standard deviation is indicative of electronic noise inherent to the measurement system. This excellent agreement between the measured and Reference values further validates the use of the

HITRAN 2012 O_2 spectroscopic parameters for exhaust measurements up to 800 K. Furthermore, the lack of any systematic drift in the measured [O_2] with T suggests the possibility of using these parameters at gas temperatures even greater than 800 K.

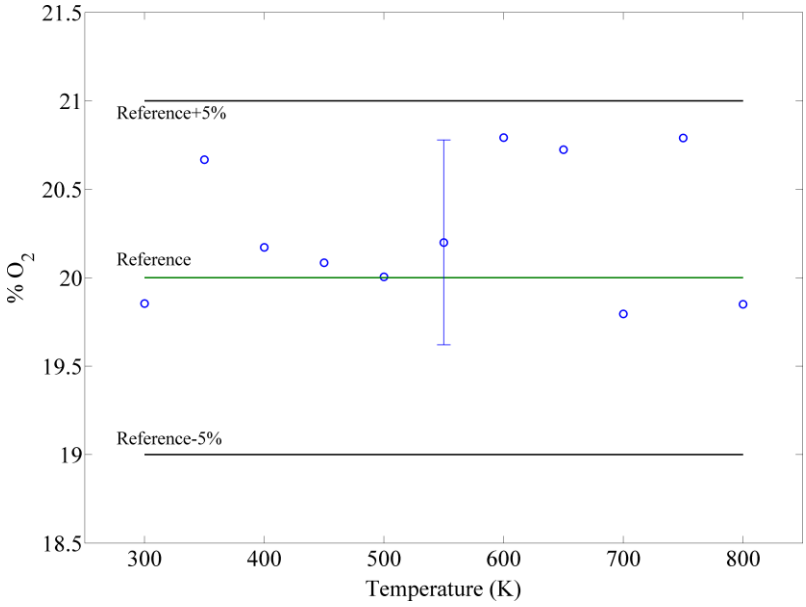

Figure 2: Good match between the actual (20-% O_2 in N_2) and measured [O_2] at gas temperatures of 300 K – 800 K. The presented results are the average of 6 independent etalon-corrected T sweeps.

4. Exhaust Oxygen Concentration Sensor Design

This section describes the design of a sensor to enable in-situ high-speed absorption-spectroscopy-base [O_2] measurements in the exhaust stream of IC engines. The multi-pass setup, which was necessitated because of very weak absorption-transition-strengths of oxygen, is discussed here along with validation of the optical-setup robustness under vibrations expected in IC-engine applications. Furthermore, T gradient considerations of using a line-of-sight setup are also discussed here. Finally, sample on-engine measurements are shown to demonstrate performance of the sensor system.

4.1 - Multi-Pass Herriott Cell for Longer Absorption Path-Length:

To compensate for the very weak O_2 absorption cross-section, a multi-pass arrangement was designed to significantly increase the absorption path length for improved signal-to-noise ratio (SNR). Specifically, a Herriott cell configuration was used to realize the multi-pass arrangement as Herriott cells provide long path lengths in a simple, stable, and compact package while being fairly immune to small perturbations that could be introduced by engine vibrations [14, 15]. The Herriott cell designed for this study utilized two 50.8-mm diameter, 200-mm focal length spherical mirrors with a common optical axis. The front or input/extraction mirror had an off-axis hole allowing for input of collimated light into the cell and extraction of the light after a certain number of passes, and the back mirror was without a hole. The hole in the front mirror was aligned with the vertical axis (x=0, y=a, z=0), where x and y are coordinates in the plane of the input/extraction mirror, ‘a’ is the distance between the mirror centerline and the

input/extraction hole, z is the dimension between the two mirrors, and the origin is the center reflective surface of the input/extraction mirror. The collimated beam launched into the cell was angled with respect to the cell axis such that it intercepts the back mirror on the horizontal axis (x=a, y=0, z=L), the beam then reflects between the two mirrors traversing an ellipse on the mirror surfaces before exiting the cell through the hole in the front mirror. The number of passes traversed by the beam before exiting the cell can be tuned by changing the spacing (z=L) between the two mirrors. For example, in this study, the mirrors were placed roughly 15 cm apart to obtain around 25 round trips of the laser light between the two mirrors before exiting the cell through the hole; for 8.5-cm single-pass absorption path length, this corresponds to 4297.4-mm multi-pass absorption path length. Once the mirror spacing was optimized for the desired absorption path length and O_2 sensitivity, the number of cell passes (and absorption path length) was immune to vibrations or small changes in the injection angle of the incident light beam as long as the mirror spacing (z=L) was maintained. Any change in Herriott-cell mode, or number of cell passes, would be apparent from a corresponding change in the measured absorption at a constant [O_2].

4.2 - Hardware Design and Analysis Methodology:

Figure 3 shows the design and final hardware of the instrumented flow section (IFS) for making high-speed exhaust [O_2] and [H_2O], gas T, and gas P measurements. The IFS serves as the sensor head or probe, and functions in conjunction with an instrument box containing lasers and detectors; the instrument box is the same used in our previous work [6,7] with a laser and detector added for O_2 spectroscopy, and is connected to the IFS via optical fibers. The IFS generally consisted of an instrumented pipe section with an attached breadboard to support external optics; in application, the IFS was inserted in the IC-engine exhaust train via standard exhaust flanges (e.g., CXRacing TRB-VBAND300-KIT-AL_1-2). The 254-mm (10-in) long and 7.62-mm (3-in) ID stainless-steel pipe section was instrumented for multi-pass optical access using 1-mm thick and 50.8-mm (2-in) diameter fused silica windows (with high-temperature anti-reflection coatings (Lattice Electro Optics (LEO) WA2-UF-WF-2004-760-High Temp), positioned with ca. 8.5-cm internal spacing, and graphite gaskets for sealing. The Herriott cell was formed by placing a 200-mm focal length concave spherical mirror with high-reflection (HR) coating outside each window; the front input/extraction mirror was an uncoated version of the ThorLabs CM508-200EH4-M02 substrate with a separate 760-nm HR coating applied (LEO-16030714); a standard mirror with broadband dielectric HR coating (ThorLabs CM508-200-E03) was used for the back mirror. The mirrors were secured in fixed, non-kinematic, mounts, and as they were not physically mounted on the hot exhaust pipe section, their spacing was maintained even at elevated temperatures; i.e., not affected by exhaust-pipe thermal expansion. With 25 round-trip passes through the Herriott cell, a total absorption path of ca. 4297.4 mm was achieved in the ca. 8.5-cm IFS multi-pass zone. A fiber collimator (ThorLabs 50-780-APC) secured in a kinematic mount was used to pitch the laser light into the Herriott cell at the desired orientation; to make this setup robust to mechanical vibrations, the standard kinematic mount was modified allowing the spring-loaded adjustment section to be locked to the base once the alignment was set. A mirror (between the pitch kinematic mount and the input/extraction mirror in Fig. 3b) directed the light beam exiting the Herriott cell onto a silicon detector (Thorlabs PDA36A) for absorption measurements. The 760-nm laser light was generated by a discrete mode laser from Eblana Photonics (EP760-DM-B), which in turn was controlled by a National Instruments data acquisition system via a Thorlabs ITC102 laser controller. All optics and the

IFS were mounted on an 18-inx6-in optical breadboard, with water-cooled flanges placed between the IFS and breadboard to mitigate breadboard heating. The entire IFS was enclosed in a metal box as shown in Fig. 3a, which was purged with N_2 to displace any ambient O_2 from the open beam path.

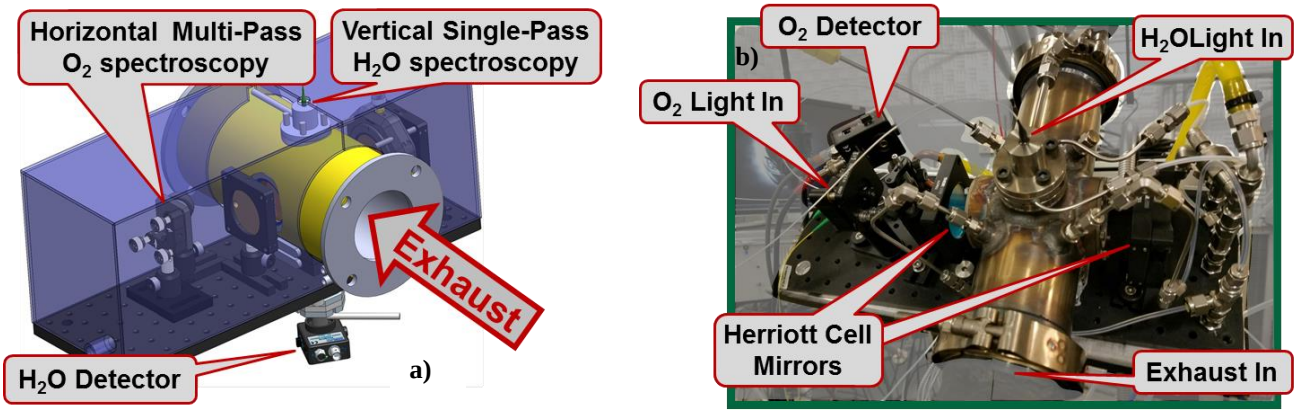

Figure 3: a) Graphic showing the general arrangement of the exhaust sensor for high-speed [O_2] and [H_2O], T, and P measurements. b) The actual exhaust sensor.

Figure 3 also shows the IFS's vertically oriented single-pass line-of-sight access for H_2O spectroscopy used to measure exhaust [H_2O], T and P. Two 12.7-mm (0.5-in) diameter fused silica wedged windows (ThorLabs WW40530) were mounted via flanges near the IFS exhaust tube ID to define the absorption pathlength. The 1388-nm laser light used for H_2O spectroscopy was pitched from the IFS top via a fiber collimator (ThorLabs 50-1310A-APC) and caught for detection on the IFS bottom via an InGaAs detector (ThorLabs PDA 20CS). The optical path outside the intended absorption path between the two wedge windows was purged with N_2 to displace any ambient H_2O from the open beam path and avoid extraneous H_2O absorption. The N_2 purge was oriented towards the wedge windows to aid in cooling the pitch collimator and catch detector; 1/4-in outside diameter (OD) tubing used for purge introduction are apparent in Fig. 3. A water-cooled heat exchanger was mounted between the IFS tube and the pitch collimator flange and is apparent with 1/8-in OD tubing supply and return lines in Fig. 3b. The longer flange necessary to span through the breadboard baseplate was sufficient to maintain suitably low detector temperature without water cooling.

Four additional NPT ports were incorporated for physical probe and guard flows as shown in Fig. 3b. The upper left port contained thermocouples and the lower two ports were used to introduce guard flows to protect the multi-pass windows from high particulate-matter (PM) transient events such as engine startup; the guard flow was introduced via 1/8-in OD tubing bent to direct the flow towards the windows. While a different design with greater flow might allow window protection with a gaseous guard flow (e.g., N_2), that was not possible with the design presented here. For several different spark-ignited (SI) IC-engine applications, using a transient guard flow of isopropanol provided suitable window protection during high-PM events. This liquid flow would sheet across the windows, completely absorbing the multi-pass light during its presence. Once the isopropanol guard flow was turned off, the residual would evaporate as the windows heated up in the hot exhaust stream, and signal from the 760-nm laser would return. Presumably other liquid guard flows would suffice, but isopropanol provided a safe, readily available, high volatility and effective guard flow for the studies described here.

Spectroscopic analysis to determine transient gas properties follows the methodology of our earlier works [3-6]; the approach is summarized here with the references providing more detail. The 760-nm and 1388-nm lasers were driven via a shifted-sawtooth waveform consisting of a zero-voltage rest period followed by a linear ramp. No laser light was emitted during the rest period, which allowed for background (e.g., interfering visible and thermal emission) detection during each cycle of the sawtooth. The laser wavelengths were ramped through the corresponding absorption transitions during the ramp section, allowing the absorption spectra to be resolved. The shifted-sawtooth waveform was modulated at 5 kHz allowing the spectra and background to be measured every 0.2 ms (1.2 crank-angle degrees (CAD) at 1000 RPM). Figure 4a shows the raw shifted-sawtooth signal for the 760-nm laser with the O_2 absorption features apparent during the wavelength ramp. After subtracting the background, portions of each O_2 and H_2O spectra were used to implement an iterative-baseline detection [3,4], which was then used to convert the signals into absorption spectra. The HITRAN parameters and approach described in Section 2 were used to analyze the O_2 and H_2O spectra and determine best-fit gas parameters. First the H_2O spectra was analyzed to determine transient [H_2O], T and P. This T and P were then used in analysis of the O_2 spectra to determine transient [O_2].

4.3 - Multi-Pass Herriott Cell Vibration Sensitivity Study:

To assess the impact of vibrations on the multi-pass Herriott cell and validate its use in the IFS for on-engine measurements, the instrument was rigidly fastened to the valve-cover of a GM 1.9-L diesel engine and absorption by ambient oxygen was monitored during engine operation. The engine was connected to a motoring-dynamometer, which could either receive or supply power to the engine; in motoring mode, it could rotate the engine at any desired speed using only electrical power and not requiring fueling and combustion within the IC engine. Figure 4a, shows O_2 wavelength-sweep scans using the shifted-sawtooth laser modulation and a 30-roundtrip-pass Herriott cell; raw detector output is shown for two measurement scans at relatively greater (blue curve) and relatively lower (red curve) Herriott cell throughput. The two major features of the shifted-sawtooth laser scan profile are illustrated in Figure 4a, including the 'laser-off' rest or background period at the scan beginning, and the nominally triangular spectral baseline shape of the remaining scan portions; time corresponds to wavelength during the ramp section. The O_2 absorption transition is apparent in the ramp sections (ca. 155 μs), and each such scan represents one temporal measurement point.

Two parameters, 'Raw Height' and '% absorption' were used to assess the IFS system's robustness to engine vibrations. The 'Raw Height' parameter indicates bulk light throughput of the Herriott cell, i.e., the absolute laser intensity coming out of the cell, and is defined here as the photodiode output at the end of the laser-scan ramp (ca. 196 μs in Fig.4a). Changing 'Raw Height' values indicate slight misalignment in the optical path across the Herriott cell from the collimator to the photodetector. Such changes can generally be tolerated as long as the absorption path length does not change dramatically; i.e. the cell mode does not change. The '% absorption' parameter is the metric relevant to gas-property measurements; this metric is the fraction of the incident light absorbed (by the absorber, O_2), and is the basis for gas-parameter calculations as outlined in Section 4.2. At a given [O_2], T, and P, the fraction of absorbed light depends only on the absorption path-length and will be constant even as the incident intensity varies; due to varying cell throughput due to e.g. cell misalignment, PM attenuation, etc. For

example, Figure 4a shows two scans with different ‘Raw Heights’ but the same ‘% absorption’ level.

The sensitivity of the Herriott cell to engine vibrations was assessed by analyzing data like in Fig. 4a, taken at 5 kHz, over a range of engine vibration extremes. Figure 4b shows fluctuations in the ‘Raw Height’ (red curve) and ‘% absorption’ (blue curve) for different engine conditions. The engine is off during the initial 1.4 s of Figure 4b, during which both the ‘Raw Height’ and ‘% absorption’ are very stable. Once the engine is motored beginning at ca. 1.4 s, significant fluctuations appear in the ‘Raw Height’ metric; as noted earlier during motoring the engine is turned by the dynamometer, and combustion does not occur. These fluctuations are indicative of dynamic Herriott-cell throughput, and a direct result of instrument shaking due to mechanical vibrations from the dynamometer spinning the 4-cylinder engine. However, despite the instrument vibration and ‘Raw Height’ variations, there is no perceivable change in the ‘% absorption’ metric relative to the engine-off condition when vibration was absent. Similarly, when engine firing (i.e. burning fuel and producing power which was absorbed by the dynamometer) began at ca. 5.1 s, while combustion significantly increased mechanical vibrations and greater ‘Raw Height’ variations, there was no perceivable change in the behavior of the ‘% absorption’ metric relative to the engine-off and motoring condition. Changes in the ‘% absorption’ metric would indicate varying absorption path-length due to vibration-induced changes in the number of Herriott cell beam passes. The absence of ‘% absorption’ variations indicates good Herriott-cell stability even when subjected to direct engine vibrations, and validates its use in the IFS for on-engine measurements. Similar results were obtained during engine operation at a range of engine speeds such as 1000, 1500, 2000 and 2500 RPM (rotations per minute).

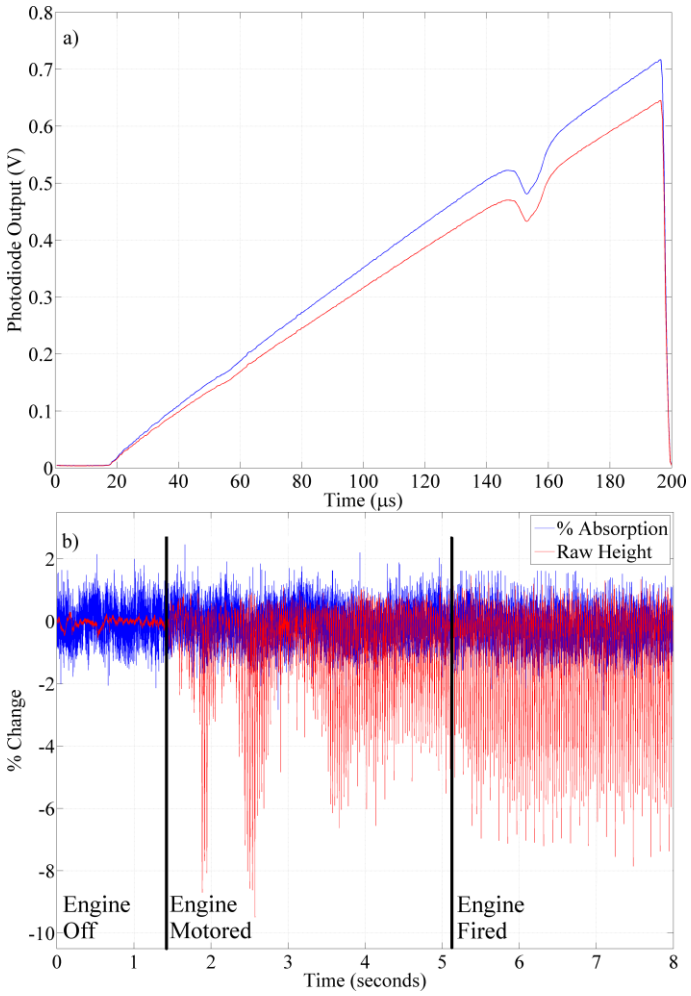

Figure 4: a) two ambient-air O_2 raw transmission scan curves with different 'Raw Heights' but same '% absorption' level. b) traces show fluctuations in the two indicated measurement parameters while the engine was off (ca. 0 to 1.4 s), motored at 1000 RPM (ca. 1.4 to 5.1 s), and fired at 1000 RPM (ca. 5.1 to 8 s). Uniformity of the '% absorption' metric across a wide range of engine vibration extremes validates the suitability of Herriott-cell based multi-pass arrangement and the IFS for measurements in vibration intensive environments and more specifically for on-engine measurements.

4.4 – Effect of Temperature Gradients Across the Absorption Path-length:

Equations (1) and (2) provide for measuring average gas properties and are valid for a measurement zone with near-uniform gas properties across the absorption path. If spatial non-uniformities in the measurement-zone gas properties exist along the absorption path, the inferred gas properties could be different from the actual path-averaged gas properties due to the non-linear dependence of absorption on both T and absorber concentration. In such situations, knowledge of gas-parameter gradient profiles could be required to accurately extract gas property information from the absorption signal. While concentration transients are common (due to engine cylinder- and cycle-specific combustion changes), spatial variations across the laser path are minimal in many application; e.g., where the sensor is several duct diameters downstream of the exhaust source. In contrast, gas T gradients across the absorption path are likely more ubiquitous and may be greater than corresponding concentration gradients due to

relatively cool exhaust duct walls and associated boundary layer effects. To evaluate the impact of such variations on gas-property measurements, the instrument was inserted in the exhaust (between the turbocharger and the three-way catalyst) of a GM 2.0-L gasoline direct injection engine operated at various steady state loads to generate a range of exhaust temperatures. The T gradient was recorded along the nominal multi-pass absorption path at various exhaust gas temperatures using a thermocouple.

Figure 5 shows the measured temperature gradients along the centerline of the Herriott cell axis (black line) as well as along a cross-section of the IFS pipe (red line); the red-line path is ca. 45° from the black-line path and was accessed via the NPT ports shown in Fig.3b. The figure shows how the Herriott cell windows are set back from the 76.2-mm IFS pipe ID creating a 85-mm window spacing and cavity at each window. Across the IFS pipe, a gradient of only ~20K was observed from the pipe centerline temperature to the gas temperature near the pipe surface. The gas temperature was observed to be near-uniform for ~80 % of the pipe radius (ca. 0-30.5 mm) and only started falling sharply beyond 85 % of the pipe radius (ca. > 32 mm) as measured from the center. However, along the nominal IFS Herriott-cell optical path, a higher ~80K gradient was observed between the pipe centerline and the optical window surface. This higher gradient could possibly be the result of flow recirculation in the window cavity and could be mitigated in future instrument modifications by moving the windows closer to the pipe ID. Despite the higher gas-temperature gradient along the Herriott cell axis, ~60 % (ca. 0-26 mm) of the Herriott cell absorption path length was observed to have near-uniform gas-temperature with a sharp temperature drop occurring primarily within the cavities (~25 % of window spacing; ca. 32-42.5 mm); i.e., 75% of the temperature gradient occurs within the cavities.

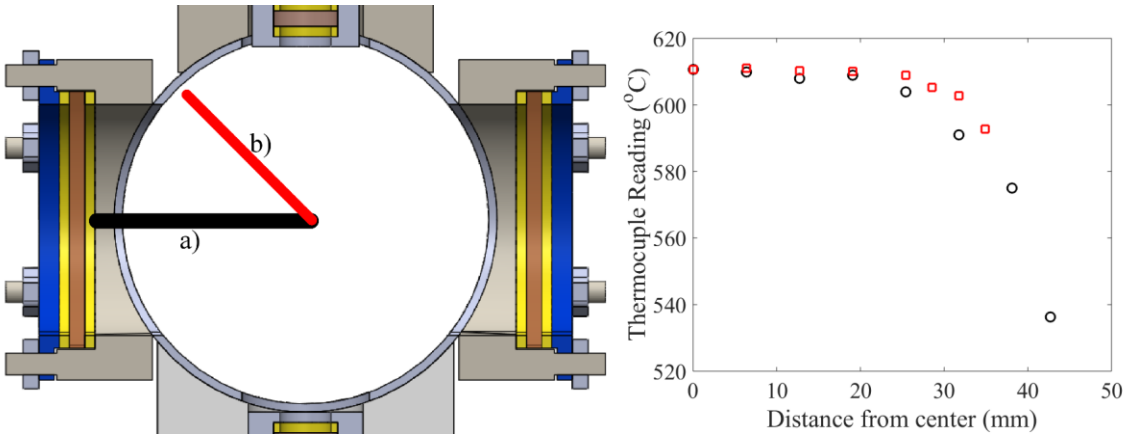

Figure 5: Black circles indicate spatial T distribution along the IFS Herriot-cell optical path (a), and red squares indicate spatial T distribution along a cross-section of the IFS pipe (b).

Based on these physical gas-temperature measurements, theoretical simulations were performed to ascertain the impact of gas-temperature non-uniformities on the gas-concentration values calculated using spectral fitting. A two-zone (hot and cold) absorption path-length model was created, and the secondary zone, which occupied 25 % of the path-length, was assigned a temperature lower than the primary zone. Theoretical spectral absorption profiles were then created for both H_2O and O_2 absorption, based on the spatially weighted temperatures of the two-zone model, and spatially uniform concentrations. Spectral fitting analysis was performed on these absorption profiles assuming spatially uniform gas properties; i.e., ignoring the gradients of

the two-zone model. Figures 6a and 6b show errors in the measured gas properties for spectral fits based on the H_2O (T, P, and $[H_2O]$) and O_2 ($[O_2]$) absorption profiles, at various hot-zone temperatures and hot-to-cold zone T differences (dT). While the parameter errors increase with increasing dT between the two model zones, the errors in $[H_2O]$ and $[O_2]$ and P are less than 1 % over the range 420-900 K for dT values up to 100 K. Figure 6 suggests that the two-zone model with dT≈50 K (i.e., 610 – (610+530)/2 = 40 ≈ 50) might best represent the case with a bulk exhaust temperature of ca. 883K (610°C), and that for this condition the related errors are negligibly low; ca. 0.15 %, 0.04 % and 0 % for $[H_2O]$, $[O_2]$, and P, respectively. For applications with significant concentration gradients, the gradients could be quantified via EGR Probe spatial mapping [6,7], and a similar multi-zone model could be used to investigate associated errors in line-of-sight analysis. This analysis shows that possible spatial T non-uniformities have insignificant effect on line-of-sight IFS measurements in engine-exhaust conditions studied here and many similar applications.

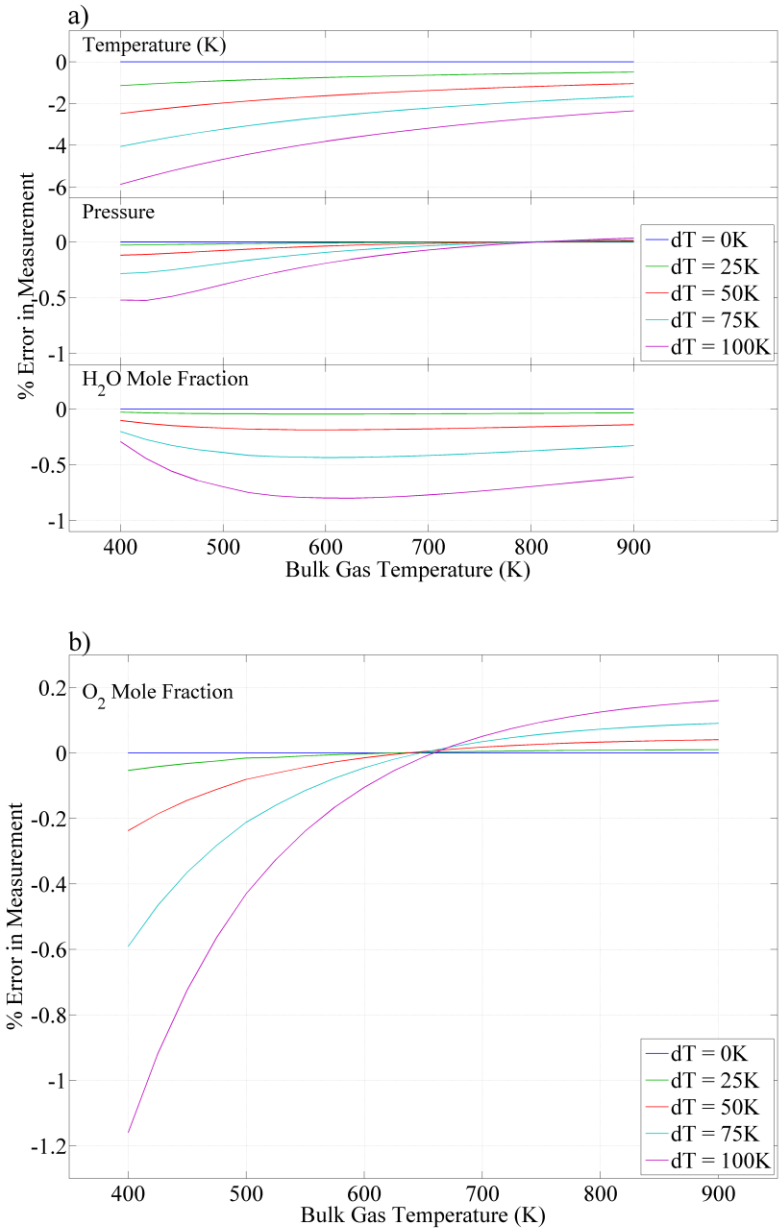

Figure 6: Impacts of spatial T gradients on measured gas properties at non-uniformity levels observed in IFS application. Gradients over a range of dT values applicable to the two-zone model are shown. (a) [H_2O], T and P. (b) [O_2]

5. Laboratory Room-Temperature Measurements

Laboratory measurements were used to characterize performance of the IFS for O_2 measurements; H_2O-spectroscopy based performance has been addressed in earlier work [3,4]. Standard mixtures of 0.2, 0.4, 0.6, 0.8, 1.2, 1.6, 2.0-% O_2 in N_2 were synthesized using a 10-point gas divider, a 2.0-% O_2 in N_2 bottled gas standard and 100 % bottled N_2 diluent. These mixtures were passed through the IFS at room T (~298 K) and 1 atm for performance analysis.

Comparison between the reference (Standard) and measured [O_2] is shown in Fig. 7. The seven red data points are the result of the IFS measurements and analysis at the corresponding standard O_2 concentrations, and the red bars indicated +/-2-σ standard deviation of mean; the measured single-shot standard deviation is ~0.05-% O_2 for all cases. The center diagonal line indicates 1:1 correspondence between the Measured and Reference axes; data points on his line have perfect accuracy. Two diagonal lines are shown indicating the region encompassed by +/-10-% variation from the center 1:1 correspondence line. The measured oxygen concentration is within 10% of the reference for all O_2 concentrations greater than 0.6 %. Based on Fig.7, the O_2 detection limit ([O_2] where SNR=1) is ca. 0.1 %, which is consistent with engine-exhaust measurements presented in the Section 6.

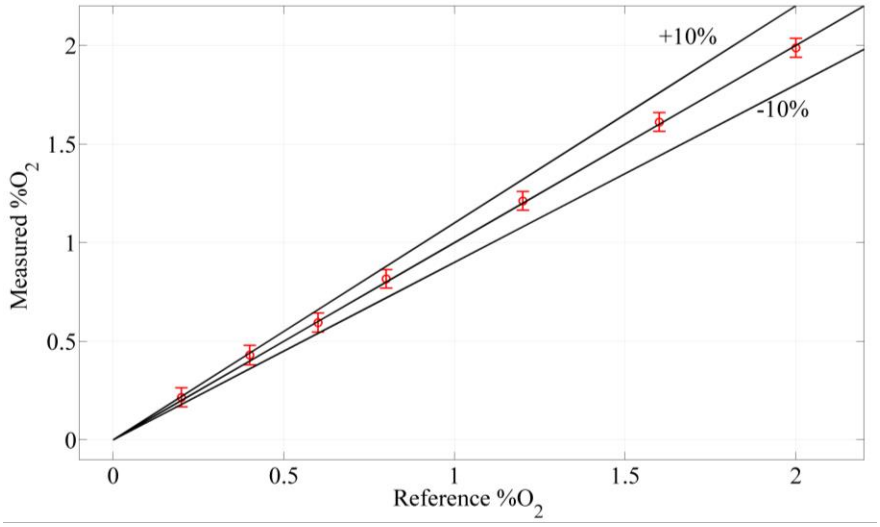

Figure 7: Oxygen calibration curve indicating measurement accuracy and precision. Measured values are within 10 % of the reference values for [O_2] ≥ 0.6 %. Tests conducted at T=298 K, P=1 atm, and L=4297.4 mm.

6. Sample On-Engine Measurements

The IFS was developed to study cylinder-to-cylinder AFR variations, enable cylinder-specific fuel tuning, and implement advanced fueling control strategies for improved combustion uniformity, and was applied to measurements on single- and multi-cylinder gasoline SI engine exhaust to advance these objectives. Figure 8 shows the IFS mounted in the exhaust train of a single-cylinder, 1.2-L, SI research engine with variable valve timing; the engine was operated with E85 (a mixture of 85-% ethanol and 15-% gasoline) for the work described here. Figure 8b shows instrument components supporting the IFS, which are similar to that used in our EGR Probe work [6,7].

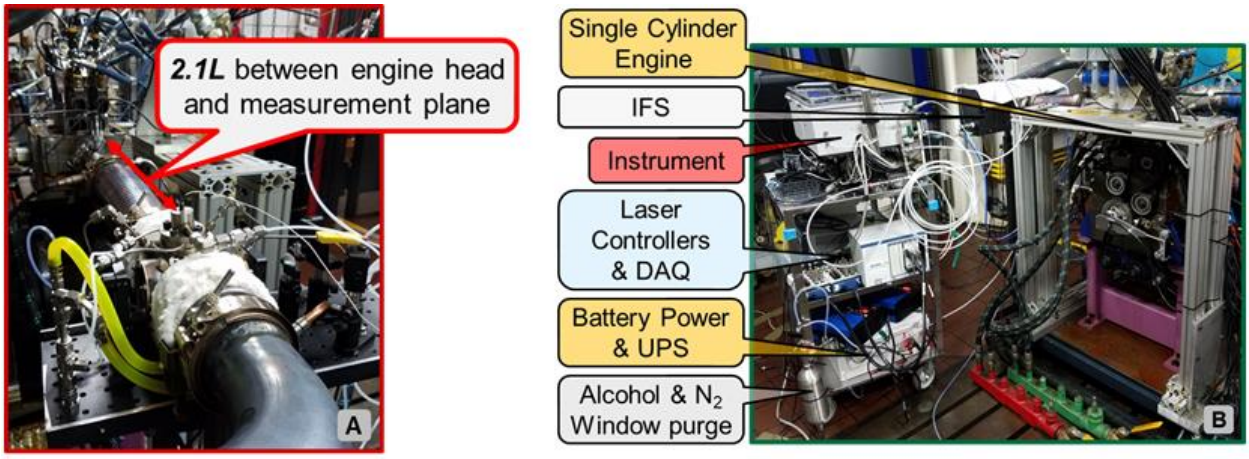

Figure 8: (A) IFS mounted in exhaust train of single-cylinder engine. (B) Instrument, IFS and engine; the Instrument contains lasers and detectors, and is connected to the IFS via optical fibers; the Laser Controllers and a data acquisition (DAQ) system are used to operate the lasers in the shifted-sawtooth 5kHz modulation and acquire the raw absorption data; Batteries are used to operate the instrument detectors to reduce noise; the isopropanol reservoir used for transient window purging is shown.

While the multi-pass approach allows detection of weakly absorbing species such as O_2 or more strongly absorbing species (e.g., H_2O, CO_2, CO, CH_4) at lower concentrations, the engine experiments demonstrated its corresponding greater sensitivity to window deposits. The isopropanol guard flow proved capable for protecting against high-PM emissions during startup, and for multi-pass window cleaning during some experiments. The single-cylinder engine experiments with E85 allowed continuous operation for over 3hrs without multi-pass window fouling. This was apparently a combined result of low PM from E85 combustion, and tight piston-ring sealing preventing oil introduction into the exhaust. Even the cycles 1&2 of Fig. 9 with unburned fuel in the exhaust, did not cause multi-pass window fouling. In applications with two different multi-cylinder engines (MCE1 & MCE2), window fouling was a greater challenge. For MCE1 operated with standard gasoline, the IFS multi-pass windows required cleaning after 20min of operation; these were relatively dry PM deposits that were not visibly obvious, and which were robust to intra-operation cleaning via the isopropanol guard flow. Exhaust O_2 measurements were not possible with MCE2 due to oil in the exhaust due to compromised piston-ring sealing; similar challenges would result from any other process that injected oil into the exhaust, such as turbocharger seal leakage. This work demonstrates the potential for further IFS improvements to mitigate window fouling; these could include shutters to block window exposure when measurements are not being made, improved guard-flow design, possibly different guard fluids or gases, or active window wipers.

Figure 9 shows IFS measured transient [O_2] and [H_2O] with the single-cylinder engine operated sequentially with and without SI in cycle pairs; i.e., no spark was provided for Cycles 1&2 (blue circles), SI occurred for Cycles 3&4 (red circles), and this cyclic process was repeated. Thus, there was no combustion for Cycles 1&2, and combustion occurred for Cycles 3&4, as apparent from the cylinder-pressure traces. Transient [O_2] and [H_2O] are indicated by the blue and red curves, respectively; the region identified as corresponding to Cycle 4 is actually from Cycle 4 of the preceding four-cycle sequence. The brackets indicate ca. one cycle width corresponding to the numerically indicated compression event; e.g., the exhaust corresponding to the combustion event 3 at ca. 210 ms occurs over the range ca. 225-300ms. There is about one-

half cycle (one TDC spacing, or one engine revolution) delay between the compression event and the corresponding measured transient for events 1&2; this is due to exhaust-valve timing, exhaust flowrate, and the ca. 2.1-L spacing (see Fig.8a) between the exhaust valve and IFS measurement plane. The combustion products of events 3&4 have higher exhaust flowrates, and the transient delay is correspondingly lower.

Figure 9 shows that [O_2] and [H_2O] transients are simultaneously measured, the species dynamics mirror each other, and that very fast transients are resolved. The individual exhaust events behave as stacked plug-flow sweeping through the downstream IFS measurement plane; a similar plug-like behavior was observed for multi-cylinder engines (not shown here). Combustion (Cycles 3&4) produces lower O_2 and greater H_2O, and fuel-rich exhaust without combustion (Cycles 1&2) produces greater O_2 and lower H_2O. Very fast transients on the order of 1 ms (ca. 9 CAD at 1500 RPM) are observed for both O_2 and H_2O, particularly at the interface of Cycles 2-3, 3-4 and 4-1. Slower mirroring intra-cycle transients are observed, and most apparent in Fig. 9 for cycles 1&2. Combustion-residual scavenging is the effectiveness with which exhaust from the previous combustion event is swept from the cylinder before the subsequent cycle, and the IFS results of Fig. 9 indicate less than perfect residual scavenging; cylinder residual can be desirable and used as internal exhaust gas recirculation (EGR). The intermediate O_2 and H_2O values for the exhaust of Cycle 1 relative to Cycles 4 and 2, is due to cylinder residual from Cycle 4 contributing to the exhaust of Cycle 1. Combustion residual from Cycle 4 still influences the exhaust of Cycle 2, and separate measurements with the single-cylinder engine (not show here) indicated that about four cycles were required to eliminate combustion residual; i.e., for this engine at the study conditions, the influence of a combustion event persists for about four cycles. Cylinder residual from Cycle 2 has a similar impact on the exhaust of Cycle 3, causing its O_2\H_2O to be greater\less than that of Cycle 4. These abilities to resolve fast inter- and intra-cycle exhaust-gas O_2 concentration and other parameter transients demonstrates the utility of the IFS for assessing engine system performance and driving development advances.

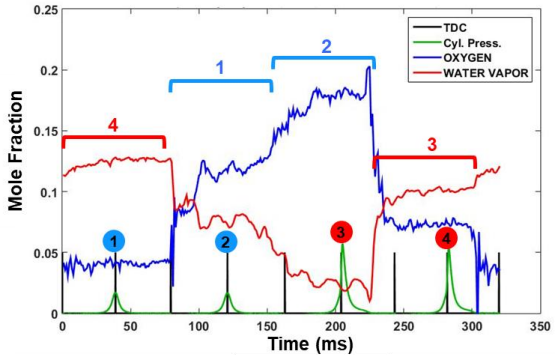

Figure 9: IFS [O_2] and [H_2O] measurements on the single-cylinder engine shown in Fig.8. Vertical black bars indicate top-dead center (TDC) as indicated by a shaft encoder, and the green curves indicate relative cylinder pressure. The four-stroke engine produces one combustion event every two TDC events. Sequential compression TDC events are numbered in the blue and red circles. The engine spark-cut skip fired in combustion-cycle pairs; no combustion occurred for events 1&2 indicated by the blue circles, and combustion occurred for events 3&4 indicated by the red circles.

7. Conclusions

We describe development and demonstration of a sensor for resolving fast [O_2] and [H_2O], T and P transients in high-temperature combustion exhaust, for applications in advancing transportation technologies. This new work focuses on the challenge of adding transient [O_2] measurements to the existing capabilities for [H_2O], T, and P measurements demonstrated in our previous work [3-6]. A multi-pass Herriott cell approach provided a solution for addressing the very weak absorption of O_2; appropriately increasing absorption path length to account for weak absorption. In addition to providing a pathway for measuring weakly absorbing species, the Herriott cell could be implemented to extend the detection limit and dynamic range of more strongly absorbing species; e.g., single and multi-pass for %-level and ppm-level H_2O and CO_2 measurements, respectively. In fact, the order or number of passes of the Herriott cell can be tuned to provide the desired sensitivity. An instrumented flow section (IFS), was developed based on single-pass line-of-sight H_2O spectroscopy, and multi-pass line-of-sight O_2 spectroscopy. The Herriott cell was shown to be immune to direct engine vibrations, making the approach applicable to engine and mobile applications; no mode hopping or significant path-length changes were observed with harsh vibration.

Exhaust gas parameters were determined based on best-fit spectral analysis of measured absorption using HITRAN spectroscopic parameters. Gas [H_2O], T and P were determined from analysis of six H_2O absorption features, and the high-temperature validity of the HITRAN H_2O parameters has been previously demonstrated. Exhaust gas [O_2] was determined from analysis of the O_2 absorption pair, and using T and P from the H_2O analysis. By analyzing absorption measurements in O_2 standards, the validity of the HITRAN 2012 O_2 spectroscopic parameters for application at temperatures up to 800K was demonstrated with less than 5-% concentration error. In room-temperature laboratory experiments, measured [O_2] above 0.6 % were accurate within 2 % of the gas standard.

Single- and multi-cylinder engine applications proved the most robust and comprehensive demonstration of the new sensor. While the multi-pass approach provides for enhanced absorption sensitivity, it has corresponding sensitivity to window deposits. An isopropanol guard flow was demonstrated to protect against high-PM startup transients, and for intra-application cleaning, and further potential design improvements to address multi-pass window fouling were discussed and recommended. Nevertheless, the IFS was capable of continuous O_2 and other exhaust parameter measurements for experiments lasting over 3 hrs for the single-cylinder engine; tight piston rings with little-to-no exhaust oil, and low-PM-producing E85 fuel. Fast ca. 1 ms (ca. 9 CAD at 1500 RPM) [O_2] and [H_2O] transients were resolved by spark-cut skip firing the single-cylinder engine, which also showed inter- and intra-cycle dynamics. These experiments also showed the ability of the IFS to resolve the efficiency of combustion-residual scavenging. The engine applications decisively demonstrated the suitability and utility of the IFS for studying cylinder-to-cylinder AFR variations, enabling cylinder-specific fuel tuning, implementing advanced fueling control strategies for improved combustion uniformity, and more general IC-engine technology advancement.

8. Acknowledgements

This research was funded by the US DOE Vehicle Technologies Office via a Cooperative Research and Development Agreement between ORNL and Cummins Inc. The authors would like to thank DOE Program Managers Gurpreet Singh and Mike Weismiller.

The authors acknowledge and thank Adam Wade, Josh Carr, Matt Meixner, Anupam Patil, Shashank Tamaskar for their contributions to the engine application described in Section 6.

This manuscript has been authored by UT-Battelle, LLC under Contract No. DE-AC05-00OR22725 with the U.S. Department of Energy. The United States Government retains and the publisher, by accepting the article for publication, acknowledges that the United States Government retains a non-exclusive, paid-up, irrevocable, world-wide license to publish or reproduce the published form of this manuscript, or allow others to do so, for United States Government purposes. The Department of Energy will provide public access to these results of federally sponsored research in accordance with the DOE Public Access Plan (http://energy.gov/downloads/doe-public-access-plan).

9. References

1. L. Ben, N. Raud-Ducros, R. Truquet, and G. Charnay, SAE Technical Paper 1999-01-2901, 1999, doi:10.4271/1999-01-2901.
2. K. Allmendinger, SAE Technical Paper 2009-01-1680, 2009, doi:10.4271/2009-01-1680.
3. G.S. Jatana, S.V. Naik, G.M. Shaver, and R.P. Lucht, International Journal of Engine Research 15(2014) 773-.
4. G.S. Jatana, M. Magee, D. Fain, S.V. Naik, G.M. Shaver, and R.P. Lucht, Applied Optics 54 (2015) 1220 – 1231
5. G.S. Jatana, S. Geckler, D. Koeberlein, and W.P. Partridge, Sensors and Actuators B: Chemical 240 (2017) 1197–1204.
6. G.S. Jatana, L. Kocher, S.-M. Moon, S. Popuri, K. Augustin, J. Helt, F. Tao, Y. Wu, R. Booth, S. Geckler, D. Koeberlein, W.P Partridge, International Journal of Engine Research, 19, No.5, (2018) 542-552.
7. N. Kawahara, E. Tomita, A. Ohtsuki, and Y. Aoyagi, Proceedings of the Combustion Institute 33(2011) 2903 - .
8. G.B. Rieker, H. Li, X. Liu, J.T.C Liu, J.B. Jeffries, R.K. Hanson, M.G. Allen, S.D. Wehe, P.A. Mulhall, H.S. Kindle, A. Kakuho, K.R. Sholes, T. Matsuura, and S. Takatanic, Proceedings of the Combustion Institute 31(2007) 3041 - 3049.
9. O. Witzel, A. Klein, C. Meffert, and S. Wagner, Opt Express 21(2013), 19951.
10. L. Kranendonk, X. An, A.W. Caswell, R.E. Herold, S.T. Sanders, R. Huber, J.G. Fukimoto, Y. Okura, and Y Urata, Optics Express 15(2007), 15115.
11. L. Ma, X. Li, S.T. Sanders, A.W. Caswell, S. Roy, D.H. Plemmons, and J.R. Gord, Optics Express 21(2013) 1152 - 1162.
12. G. Rieker, J. Jeffries, R. Hanson, T. Mathur, M. Gruber, and C. Carter, Proceedings of the Combustion Institute 32(2009) 831 - 838.
13. R.M. Mihalcea, D.S. Baer, and R.K. Hanson, Symposium (International) on Combustion 27(1998) 95 – 101.
14. D. R. Herriott, H. Kogelnik, R. Kompfner, Appl. Opt. 3 (1964) 523.
15. J. B. McManus, P. L. Kebabian, M. S. Zahniser, Appl. Opt. 34 (1995) 3336.

16. H. E. Schlosser, J. Wolfrum, V. Ebert, B. A. Williams, R. S. Sheinson, and J. W. Fleming, Proceedings of the Combustion Institute, ISSN: 1540-7489, Vol: 29, Issue: 1, Page: 353-360 (2002). DOI: 10.1016/s1540-7489(02)80047-5
17. Z.-R. Zhang, P.-S. Sun, H. Xia, Z. Li, T. Pang, B. Wu, X.-J. Cui, and F.-Z. Dong, J. Opt. Technol. 83, 673-677 (2016). https://doi.org/10.1364/JOT.83.000673
18. S. Neethu; R. Verma; S. S. Kamble; J. K. Radhakrishnan; P. P. Krishnapur; V. C. Padaki, Sensors and Actuators B: Chemical, Vol: 192, Page: 70-76. (2014). http://dx.doi.org/10.1016/j.snb.2013.10.070
19. Y. B. Wei; J. Chang; J. Lian; T. Y. Liu, Optik, Vol: 126, Issue: 20, Page: 2394-2397 (2015) http://dx.doi.org/10.1016/j.ijleo.2015.06.013
20. P. Vogel, V. Ebert, Appl. Phys. B 72, 127–135 (2001) DOI: 10.1007/s003400000516
21. X. Zhou; J. Yu; L. Wang; Q. Gao; Z. Zhang, Sensors and Actuators B: Chemical, Vol: 241, Page: 1076-1081 (2017). http://dx.doi.org/10.1016/j.snb.2016.10.033
22. L.S. Rothman, D. Jacquemart, A. Barbe, D.C. Benner, M. Birk, L.R. Brown, et al., J. Quant. Spectrosc. Radiat. Transf. 96 (2005) 139 - 204.
23. X. Liu, X. Zhou, J. B. Jeffries, and R. K. Hanson, J. Quant. Spectrosc. Radiat. Transf. 103 (2007) 565–577.
24. Krupenie, Paul H. J. Phys. Chem. Ref. Data. 1(1972) 423–534.
25. L.S. Rothman, I.E.Gordon, Y.Babikov, A.Barbe, D.ChrisBenner, P.F.Bernath, et al., J. Quant. Spectrosc. Radiat. Transf. 130 (2013) 4–50.

10. Biographies

Dr. Gurneesh Singh Jatana completed his PhD from Purdue University in 2014 and performed this research work while working as a post-doctoral research scholar at Oak Ridge National Lab. His research interests included absorption-spectroscopy-based gas property sensors and their application for measurements on production spec. multi-cylinder I.C. engines to provide high-speed data for CFD model validation/tuning and control model development. He also has considerable experience with low-speed-pre-ignition as well as dilute combustion in spark ignited engines. He is currently working at Cummins Inc. as an engine performance development senior engineer.

Mr. Anthony Perfetto graduated with a BS and MS from Purdue University in 2004 and 2009. He currently works in Cummins Product Development and has more than 14 years of powertrain development experience. His work assignments include engine performance team leader roles in diesel systems, system integration leader for Cummins Advanced spark ignited development work, system performance lead in product development. He holds several patents in the area of powertrain development.

Mr. Sam Geckler earned Bachelor and Masters of Mechanical Engineering from Purdue University in 1992 and 1994 respectively. He joined powertrain consulting group FEV in 1994 and held engine performance development roles in alternative fuels programs, diesel combustion system design and after-treatment integration. Since 2002, he has been with Cummins Inc. At Cummins, he was the engine performance leader for the 2007 RAM truck program launching the first Heavy Duty truck using NO_x adsorber technology, and more recently he was the program

leader for the Cummins ETHOS program demonstrating high efficiency spark ignited engine concepts based upon low carbon fuels.

Dr. W. P. Partridge completed his PhD work at Purdue University in 1995, and is currently Distinguished Research Staff at Oak Ridge National Laboratory (ORNL). His research focuses on developing and applying robust, practical and field-deployable diagnostics to advance transportation technologies, with specific emphasis on combustion, catalysis, and engine systems; these have contributed to several significant Cummins advances including the 2015 5-L V8 (Nissan Titan), the SuperTruck and 2007 6.7-L ISB (Dodge Ram). He was recognized as ORNL's 2008 Distinguished Engineer, and received the 2010 Outstanding Mentor Award from the US DOE Office of Science for his work with students and post-graduates.